PHYSICAL MECHANISMS GOVERNING DEPOSITION RATE IN ARC WELDING WITH A CONSUMABLE ELECTRODE

P. F. MENDEZ*, Z. YAN**, V. NÚÑEZ SÁNCHEZ*, S. CHEN**

*Canadian Centre for Welding and Joining, University of Alberta, Canada
**Beijing University of Technology, China

DOI 10.3217/978-3-85125-968-1-05

ABSTRACT

This paper presents a model of deposition rate in gas metal arc welding (GMAW). Some aspects of this model are also helpful to understand related processes such as MCAW, FCAW, SAW, SMAW, EGW, ESW and how-wire additions. Deposition rate is one of the essential factors in calculation of welding costs and times to completion in practical applications. The relationship of deposition rate with current is also determinant of dilution of deposited material (essential concept in overlays) and is a tool of diagnostic of the welding process. For some common materials such as aluminum alloys, the variations in deposition rate with current are not well understood, and common explanations might be misleading. The foundations of the model are mass and energy balances together with the mass and heat transfer mechanisms involved. Heat transfer mechanisms considered include the energy deposited by the fall voltage of the arc against the consumable, Joule heating of the electrode extension, evaporation losses, and heat exchange with the contact tip. The calculation of Joule heating considers the amount and shape of electrical resistivity variation with temperature. The approach presented is in contrast with the common use of company literature for the relationship between current and wire feed speed, or with the use of a second order expression with tabulated constants specific for particular materials and process configurations. The model developed allows to predict the effect of electrode extension and droplet temperature, which are not explicit in current approaches.

Keywords: arc welding, droplet temperature, deposition rate

INTRODUCTION

Wire-fed processes have the unique property that deposition rate and penetration are coupled, since both are controlled by the same current. The knowledge of the relationship between current and wire feed speed is essential for the determination of welding procedures and is provided in commercial consumable literature.

Commercial literature, however, does not capture the effect of electrode extension and shielding gas. More importantly, when commercial literature is not available, trial and error is the only practical resource left. Much of the commercial literature is now migrating to apps created by the suppliers, yet novel or unusual alloys are not covered in the apps either. The problem of determining procedures using novel consumables is

especially relevant in wire arc additive manufacturing (WAAM), which involves alloys seldom used in welding such as titanium and Inconel.

Attempts to generalize the relationship between current and deposition rate include the use of expressions such as [1]

$$\dot{m} = C_1 I + C_2 I^2 \quad (1)$$

where C_1 and C_2 are empirical constants determined for a given consumable. The problem is again, for new alloys without these empirical constants, there is no guidelines for procedure development. An understanding of the relationship between current and deposition rate will also yield light into droplet temperature, which is one of the main parameters determining fume formation.

Past work has focused on the mass and energy balance during deposition rate, in GMAW early work was done by Lesnewich [1], Halmoy [2], and Waszink [3]. More modern references include [4–6]. In all these cases, knowledge of droplet temperature and vaporization rate are needed, but not available.

This work aims to extend previous efforts by incorporating measured values of droplet temperature and estimating vaporization rates and metal transfer geometries with more detail than any previous research.

EXPERIMENTS

Droplet temperature was measured using the setup described in [8] illustrated in Fig. 2, and the techniques developed in [9–14]. The values of wire feed speed for steel and pure iron are illustrated in Fig. 1, showing a good match with the tabulated values in [7], but also showing a lower wire feed speed in pure Fe electrode that could not be anticipated.

The values of droplet temperature obtained are illustrated in Fig. 3. the trends obtained are consistent with all previous observations, featuring a “dip” at the point of transition from globular to spray transfer. It is interesting to observe that the droplet temperature in aluminum alloys decreases greatly with the amount of Mg present in the alloy, as first identified in [8]. Similarly, ER80S-G, which contains the high vapor pressure element Mn, displays a lower droplet temperature than the pure iron electrode.

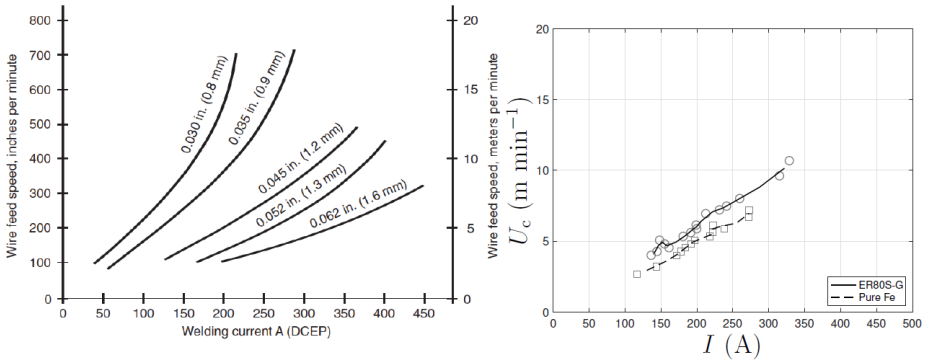

Fig. 1 Left: Typycal representation of current and wire feed speed in solid-steel wire in the commercial literature [7]. Right: Measurements of 1.2 mm wire in experiments performed.

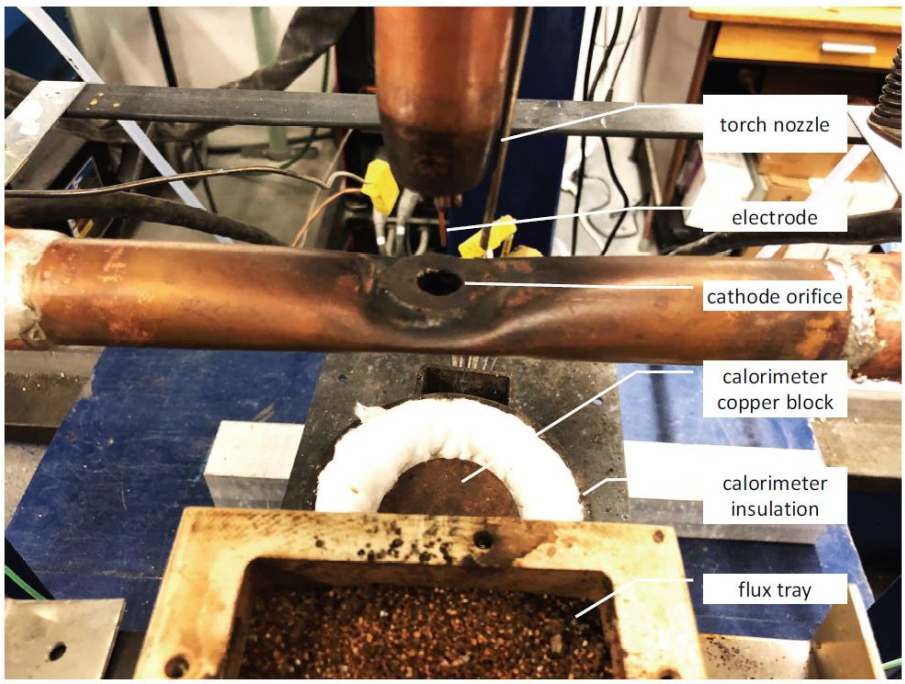

Fig. 2 Experimental setup for measuring droplet temperature [8]

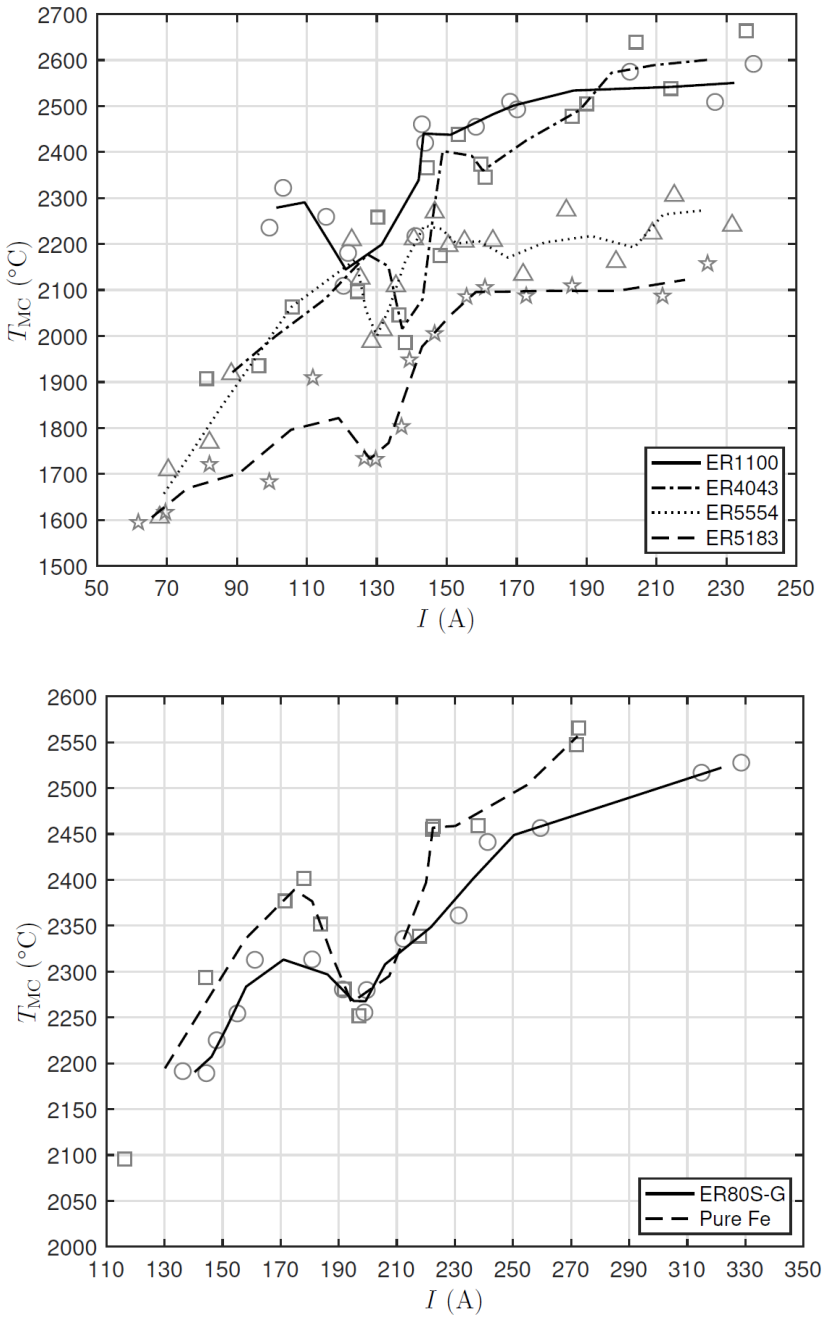

Fig. 3 Droplet temperature in experiments performed. Markers indicate independent measurements, and trendlines correspond to a moving average of two points.

MASS BALANCE

Consider a melting wire in GMAW with free-flight transfer, as illustrated in Fig. 4. Consider times t_1 and t_2 corresponding to similar stages of two different droplet detachments. The time interval between t_1 and t_2 contains a large number of detachment cycles.

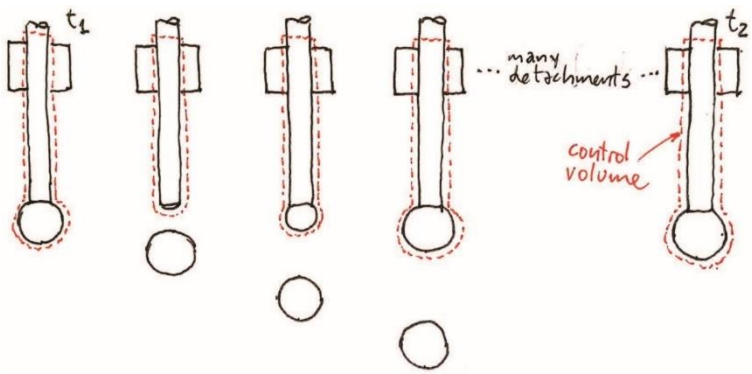

Fig. 4: Sequence of droplet detachments in a time interval.

A mass balance between t_1 and t_2 in the control volume indicated in Fig. 4 establishes:

$$m_{\text{in}} = m_{\text{out}} \tag{2}$$

where m_{in} and m_{out} are the mass that entered and left the control volume between times t_1 and t_2. The average mass rate between t_1 and t_2 can be calculated as

$$\dot{m} = \frac{m}{t_2 - t_1} \tag{3}$$

resulting in

$$\dot{m}_{\text{in}} = \dot{m}_{\text{out}} \tag{4}$$

The notation stands for a time average mass rate, it is not an instantaneous value.

MASS ENTERING THE CONTROL VOLUME

The mass rate entering the control volume is given by the wire feed speed and wire cross section. This equation is valid for processes with constant wire feed speed such as standard GMAW or CV-SAW, and variable wire feed speed such as CC-SAW or Fronius MCT GMAW.

$$\dot{m}_{\text{in}} = \dot{m}_{\text{C}} = \rho_{\text{C}} A_{\text{C}} U_{\text{C}} \tag{5}$$

where ρ_{C} are the density, A_{C} cross sectional area, and feeding speed of the wire.

MASS LEAVING THE CONTROL VOLUME

The mass exiting the control volume does it either as molten metal (in the form of droplets and spatter), and metal vapors evaporated from the surface of the droplet:

$$\dot{m}_{\mathrm{out}} = \dot{m}_{\mathrm{MC}} + \dot{m}_{\mathrm{V}} \tag{6}$$

For the steel experiments performed, the estimated amount of vaporized metal is always below 1% by mass, while for the aluminum experiments, for the Mg-containing alloys it was estimated as reaching up to about 4%.

OVERAL MASS BALANCE

The overall heat balance is obtained by combining equations 4, 5, and 6:

$$\dot{m}_{\mathrm{C}} - \dot{m}_{\mathrm{MC}} - \dot{m}_{\mathrm{V}} = 0 \tag{7}$$

ENERGY BALANCE IN GMAW

Similarly as with mass balance, consider the same control volume, and times t_1 and t_2 in Fig. 4 corresponding to similar stages of two different droplet detachments. Because the thermal expansion in the solid or molten metal and the heat generated by viscous dissipation are very small, the conversion between mechanical and thermal energy is negligible in either direction, and the energy balance is in practice a heat balance.

An energy balance in the control volume between t_1 and t_2 establishes:

$$Q_{\mathrm{in}} - Q_{\mathrm{out}} + Q_{\mathrm{gen}} = Q_{\mathrm{st}} \tag{8}$$

where Q_{in} and Q_{out} are the thermal energies that entered and left the control volume between times t_1 and t_2. Q_{gen} is the amount of heat generated inside the control volume, and Q_{st} is the amount of thermal energy stored inside the control volume during the time interval.

Because at times t_1 and t_2 the control volume contains wire and droplets at the same stage of detachment, the amount of thermal energy contained inside the control volume is the same, so the amount of heat stored between t_1 and t_2 is

$$Q_{st} = 0 \tag{9}$$

An average heat rate between t_1 and t_2 can be calculated as

$$q = \frac{Q}{t_2 - t_1} \tag{10}$$

resulting in the following overall energy balance:

$$q_{\mathrm{in}} - q_{\mathrm{out}} + q_{\mathrm{gen}} = 0 \tag{11}$$

which also accounts for the absence of heat stored. Similarly as before, the notation stands for a time average heat rate, not an instantaneous value.

HEAT ENTERING THE CONTROL VOLUME

The heat rate entering the control volume is given by five components: advection by the incoming wire q_{advin}, heat from the arc column towards the electrode $q_{\text{AC,C}}$, heat conducted from the contact tip to the consumable $q_{\text{CT,T}}$, heat generated by the electrical resistance at the point of contact with the contact tip $q_{\text{CT,C}}$, and overall fall voltage q_{Cfall} on the surface of the electrode. The heat generated by the contact tip contact resistance and the heat generated by the fall voltage are considered to be created at the surface of the electrode:

$$q_{\text{in}} = q_{\text{adv}_{\text{in}}} + q_{\text{AC,C}} + q_{\text{CT,C}} + q_{\text{C}_{\text{cont}}} + q_{\text{C}_{\text{fall}}} \tag{12}$$

HEAT LEAVING THE CONTROL VOLUME

The heat rate leaving the control volume is given by two components: advection by the molten metal and by metal vapors q_{advout} and heat lost towards the environment $q_{\text{C,env}}$:

$$q_{\text{out}} = q_{\text{adv}_{\text{out}}} + q_{\text{C,env}} \tag{13}$$

HEAT GENERATED INSIDE THE CONTROL VOLUME

The heat rate generated inside the control volume is given by the heat generated by Joule heating in the electrode extension q_{EE}.

$$q_{\text{gen}} = q_{\text{EE}} + q_{\text{MC}_{\text{Joule}}} \tag{14}$$

OVERALL HEAT BALANCE

The overall heat balance is obtained by combining equations 11, 12, and 13:

$$q_{\text{adv}_{\text{in}}} + q_{\text{AC,C}} + q_{\text{CT,C}} - q_{\text{adv}_{\text{out}}} - q_{\text{C,env}} + q_{\text{EE}} + q_{\text{C}_{\text{cont}}} + q_{\text{C}_{\text{fall}}} + q_{\text{MC}_{\text{Joule}}} = 0 \tag{15}$$

$$q_{\text{adv}_{\text{tot}}} + q_{\text{AC,C}} + q_{\text{CT,C}} - q_{\text{C,env}} + q_{\text{EE}} + q_{\text{C}_{\text{cont}}} + q_{\text{C}_{\text{fall}}} + q_{\text{MC}_{\text{Joule}}} = 0 \tag{16}$$

where

$$q_{\text{adv}_{\text{tot}}} = q_{\text{adv}_{\text{in}}} - q_{\text{adv}_{\text{out}}} \tag{17}$$

For the steel experiments performed, 80% to 90% of the heat comes was estimated to come from the anode fall voltage, and about 10% from the electrode extension. For the aluminum experiments performed, 90% to 95% came from the anode fall voltage, with

about 1% of the heat coming from the electrode extension. The consumable loses heat to the environment by the mechanisms of convection and radiation, which were determined to be negligible under typical conditions [15].

METAL TRANSFER GEOMETRY

Metal transfer in free-flight has several different configurations [16, 17]. For the droplet temperature measurements performed, we will consider two representative geometries, illustrated in Fig. 5. This simplification is made acknowledging future work should be able to capture further subtleties, such as the presence of a molten tail in streaming spray transfer.

In the geometry considered, d_{MC} is the droplet diameter and $L_{\mathrm{AC,C}}$ is the attachment of the arc to the electrode. The size of this attachment is a property of the arc, and there are currently no guidelines on how to predict it. In this work, it will be approximated based on experience as

$$L_{\mathrm{AC,C}} = d_{\mathrm{C}}/2 \tag{18}$$

In solid wire processes, the droplet diameter is often estimated from droplet detachment frequency, neglecting the mass lost to evaporation in Eq. 7:

$$d_{\mathrm{MC}} = \left(\frac{3}{2}\frac{\rho_{\mathrm{C}}}{\rho_{\mathrm{MC}}}\frac{U_{\mathrm{C}}{d_{\mathrm{C}}}^{2}}{f_{\mathrm{MC}}}\right)^{1/3} \tag{19}$$

The area of attachment of the arc to the droplet, in the case of globular transfer is approximated as

$$A_{\mathrm{AC,C}} = \pi {L^2}_{\mathrm{AC,C}} \tag{20}$$

The detachment frequency in the experiments was measured approximately and only in some experiments. An empirical fit based on welding current was generated.

$$f_{\mathrm{MC}} = \begin{cases} C\ I & for\ I \le I_{\mathrm{C}} \\ A\ I - B & for\ I > I_{\mathrm{C}} \end{cases} \tag{21}$$

where I_c, A and B are constants determined empirically, and $C = A\ B/I_c$. For the case of a pure Fe consumable, the detachment frequency was not measured, but it is assumed to be the same as in ER80S-G, with f_{MClow} =50 s^{-1}, A =1.565 $s^{-1}A^{-1}$, B =231.8 s^{-1}, and I_c =180 A. The detachment frequency of all aluminum wires was similar, and the same empirical expression is used for all, with with f_{MClow} =25 s^{-1}, A =2.688 $s^{-1}A^{-1}$, B =319.9 s^{-1}, and I_c =128 A. The droplet diameters estimated for the experiments performed are between 0.95 and 2 times the wire diameter.

COMPONENTS OF MASS BALANCE

TOTAL MASS EVAPORATED

The total mass evaporated is the sum of vaporization of all components of the alloy:

$$\dot{m}_{\mathrm{V}} = \sum_j \dot{m}_{\mathrm{V}_j} \tag{22}$$

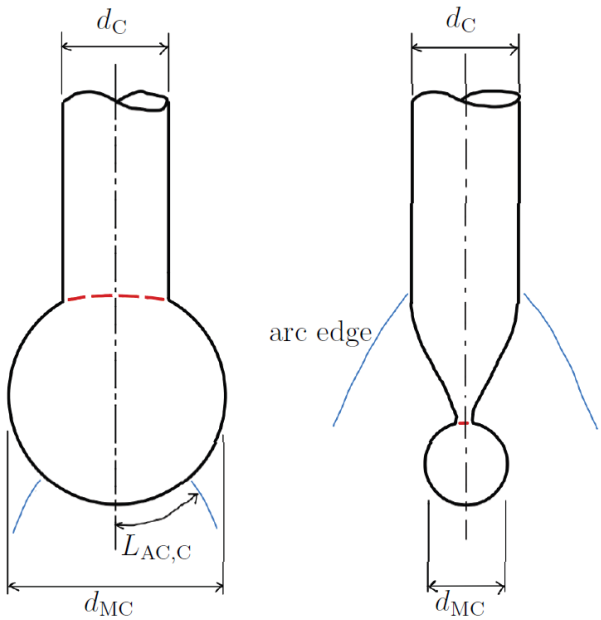

Fig. 5 Representative configurations for globular (left) and spray transfer (right)

where $\dot{m}_{V_j}$ is the mass rate of evaporation of each alloying element, e.g. Fe, Mn, etc. in steels, or Al, Mg, etc. in many aluminum alloys. Because of the different vapor pressures of each alloying component, evaporation does not follow the stoichiometry of the melting electrode. For the case of steel wires containing 1.7 wt% Mn, about 55 wt% to 75 wt% of welding fumes are Mn, the rest is Fe, with negligible amounts of other alloying elements. For the case of aluminum, the Mg-containing alloys, Mg can also make up to 75 wt% of their fumes, the rest Al, with negligible amounts of the other alloy components.

EVAPORATION KINETICS

In an alloy, the evaporation of each component is proportional to its mass flux and area of evaporation:

$$\dot{m}_{\mathrm{V}_j} = \dot{m}''_{\mathrm{V}_j} A_{\mathrm{MC}} \tag{23}$$

while the mass flux of each component is proportional to the partial vapor pressure of the component and inversely proportional to the resistance to mass transfer it encounters

$$\dot{m}''_{\mathrm{V}_j} = \frac{M_j p_{\mathrm{lg}_j}}{R\, T_{\mathrm{MC}_{surf}}} \frac{1}{\Re''_{tot_j}} \tag{24}$$

The partial vapor pressure of the component is proportional to the activity in the alloy [18]

$$p_{lg_j} = a_j\, p_{\mathrm{lg}_{\mathrm{pure\,j}}} \tag{25}$$

Where $p_{lg_{pure\,j}}$ is the equilibrium vapor pressure of element *j* in pure state. In this case, we will approximate the activity a_j using Raoult's law:

$$a_j = f_{mol_j} \tag{26}$$

The vapor pressure of the component is typically tabulated as:

$$\log p_{lg_{pure\,j}} = A + \frac{B}{T_{MC_{\mathrm{surf}}}} + C \log T_{MC_{surf}} + D\, T_{MC_{surf}} 10^{-3} \tag{27}$$

with the values of *A*, *B*, *C*, *D* listed in [19], with a special treatment for Si from [20]. The magnitudes $\dot{m}''_{\mathrm{V}_j}$,which depends on droplet temperature, and A_{MC} vary as the droplet forms between successive detachments. In the calculations performed, T_{MCsurf} will be assumed to be the average temperature of the droplet just before detachment and A_{MC} the electrode tip geometry just before detachment.

The total resistance to mass transfer of component *j* as having three components: resistance to diffusion through a boundary layer of alloy depletion on the surface of the melt, ($\Re_{\mathrm{lj}}$), resistance to evaporation under a partial pressure of vapor *j* ($\Re_{\mathrm{lg,j}}$), and resistance to diffusion through a boundary layer in the gas phase, outside which the partial pressure of vapor *j* is 0.

$$\Re''_{tot_j} = \Re''_{l_j} + \Re''_{lg_j} + \Re''_{v_j} \tag{28}$$

with

$$\Re''_{l_j} = \frac{1}{h_{l_j}} \tag{29}$$

$$\Re''_{lg_j} = \sqrt{\frac{2\pi M_j}{R T_{MC_{surf}}}} \tag{30}$$

$$\Re''_{v_j} = \frac{1}{h_{v_j}} \tag{31}$$

where *h* indicates the convection coefficients for mass transfer. The mass transfer resistance of the solvent in the molten consumable (e.g. Fe in steels consumables and Al in aluminum alloys) has a resistance $\Re''_{l_{solvent}} = 0$.

In steels, the dominant resistance to evaporation is the vapor boundary layer, with approximately 95% of total resistance for Fe, and 85% for Mn. The resistance to mass transfer of Mn in the alloy-depleted melt surface is approximately 10%. In aluminum alloys, the vapor boundary layer is dominant for Al (97%) and Mg (80%), the resistance to mass transfer of Mg in the liquid is of the order of 17%. In all cases, the resistance to evaporation at the surface (R_{lg}'') is below 10%. This is an important finding indicating the importance of boundary layers in mass loses by evaporation, which are often omitted in the welding literature.

Diffusion in the melt

For the melt near the surface, being a free surface, the characteristic velocity of the fluid is not affected by a viscous boundary layer, and mass transfer parameters can be estimated as

$$h_{l_j} = \frac{Sh_{MC_j} D_{MC_j}}{d_{MC}} \tag{32}$$

$$\mathrm{Sh}_{MC_j} = 2 + 0.5\,\mathrm{Re}_{d_{MC}}^{1/2}\mathrm{Sc}_{MC_j}^{1/2} \tag{33}$$

$$Re_{d_{MC}} = \frac{U_{MC} d_{MC}}{\nu_{MC}} \tag{34}$$

$$Sc_{MC_j} = \frac{\nu_l}{D_{MC_j}} \tag{35}$$

where D_{MCj} is the diffusivity of component *j* in the melt, U_{MC} is the characteristic velocity of molten metal inside the droplet, and ν_{MC} is the kinematic viscosity of the molten metal at the bulk temperature of the droplet T_{MC}. The constant 2 accounts for mass transfer by static diffusion.

The range of $\mathrm{Sh_{MC}}$ spans from orders of 10^1 to 10^3 in steels and aluminum alloys, indicating that convection dominates over molecular diffusion in the liquid in most cases. The range of $\mathrm{Sc_{MC}}$ spans from orders of 10^1 to 10^5 in steels and aluminum alloys, indicating that the diffusion occurs in a much narrower range than momentum transport in the liquid.

Diffusivities in the liquid are typically expressed as $D_{MC_j} = D_{0_j} exp[-Q_j/(RT)]$ tabulated in [21] for steels, in [22,23] for aluminum, and also in [24,25] for more base alloys. The temperature used for diffusivity and kinematic viscosity is that of the surface of the molten metal, $T_{MC_{surf}}$.

The velocity of melt in globular transfer can be estimated roughly from [3] as shown below, with $K = 2 10^{-3}$ m s^{-1}A^{-1}:

$$U_{MC} = KI \tag{36}$$

Diffusion in the gas

For mass transfer in the gas phase, two cases must be considered: evaporation in an inert atmosphere such as GMAW of aluminum alloys using pure Ar shielding, and evaporation in a reactive atmosphere such as GMAW of steel alloys using Ar-O_2 or Ar-CO_2 shielding. In this paper we consider only the first case. In the second case, the reaction reduces the thickness of the boundary layer, resulting in increased evaporation [26,27] and fumes formation [28,29]. The association of carbon with oxygen on the surface of the melt results in an energy source that might be significant, and also on decarburization of the melt.

For the case of diffusion of metal vapors in an inert atmosphere, the convection coefficient for mass transfer can be estimated using the common correlation for convection around spheres [30], also used in [31].

$$h_{V_j} = \frac{Sh_{AC_j} D_{AC_j}}{d_{MC}} \tag{37}$$

$$Sh_{AC_j} = 2 + 0.6\, Re_{AC}^{1/2}\, Sc_{AC_j}^{1/3} \tag{38}$$

$$Re_{AC} = \frac{U_{AC} d_{MC}}{\nu_{AC}} \tag{39}$$

$$Sc_{AC_j} = \frac{\nu_{AC_j}}{D_{AC_j}} \tag{40}$$

where ν_{AC} is the kinematic viscosity of the plasma and D_{AC_j} is the diffusivity of vapor element j in the plasma. Both properties are evaluated at a "film temperature" intermediate between the molten surface (of the order of 3000 K for the case of steel and aluminum) and the plasma temperature outside the plasma boundary layer near the surface of the electrode (of the order of 7300 K for the case of Ar, resulting in a "film temperature" of approximately 5000 K). The kinematic viscosity and other thermophysical properties for the plasma are provided, for example in [32]. Typical values of Sh_{AC_j} are around 10^1, indicating convection is dominant. Typical values of Re_{AC} are of the order of 10^2. Schmidt numbers in the vapor are around 1.5.

The velocity in the arc column U_{AC} can be estimated as [33]:

$$U_{AC} = \frac{1}{2}\sqrt{\frac{\mu_0 I J_{AC,MC}}{\pi \rho_{AC}}}\, f_{U_{AC}} \tag{41}$$

where μ_0 is the magnetic permeability of vacuum, $J_{AC,MC}$ is the current density of the arc attachment with the electrode, and ρ_{AC} is the density of the plasma at approximately 10000 K, also from [34]. The velocities predicted are of the order of 200 ms^{-1}, consistent with typical plasma arc velocities.

The plasma current density can be approximated as

$$J_{AC,MC} = \frac{I}{\pi\, L_{AC,MC}^2} \tag{42}$$

where $L_{AC,MC}$ is the radius of arc attachment, which will be approximated as half the consumable diameter; this rough approximation is consistent with the analysis in [3]. The correction factor $f_{U_{AC}}$ is

$$f_{U_{AC}} = 0.55\left(\frac{\widehat{Re}_{AC}}{4}\right)^{0.073}\left(\frac{2L_{arc}}{d_C}\right)^{0.0068} \tag{43}$$

Where $\widehat{Re}_{AC}$ is a nominal Reynolds number calculated using Eq. 41 without the correction factor $f_{U_{AC}}$.

Diffusivity in plasmas is very complex [35], and it will be approximated here as diffusion in the gas phase using the Chapman-Enskog theory [36]

$$D_{Ar,j} = \frac{A\,T^{3/2}}{p\sigma_{Ar,j}^2\Omega_j M_{Ar,j}^{1/2}} \tag{44}$$

where $D_{Ar,j}$ is the diffusivity of vapor element j in Ar in cm s^{-2}, A =2.6610^{-3}, p is the atmospheric pressure in bar, σ is the effective cross section of atoms in Å, $M_{Ar,j}$ is

$$M_{Ar,j} = 2\left(\frac{1}{M_{Ar}} + \frac{1}{M_j}\right)^{-1} \tag{45}$$

where M is the molar weight of gases and vapors involved, and $\boldsymbol{\Omega}_j$ is given by [36]:

$$\Omega_j = \frac{1.06036}{T_j^{*0.15610}} + \frac{0.193}{exp\left(0.47633\,T_j^*\right)} + \frac{1.03587}{exp\left(1.52996\,T_j^*\right)} + \frac{1.76474}{exp\left(3.89411\,T_j^*\right)} \tag{46}$$

where the value of T_j^* is provided by [27]

$$T_j^* = \frac{kT_{film}}{\epsilon_{Ar,j}} \tag{47}$$

$$\epsilon_{Ar,j} = \sqrt{\epsilon_{Ar}\epsilon_j} \tag{48}$$

$$\sigma_{Ar,j} = \frac{\sigma_{Ar}+\sigma_j}{2} \tag{49}$$

where ϱ is the parameter of a Lennard-Jones potential for each component, and it is tabulated. The area from which evaporation happens will be approximated as

$$A_{MC} = \pi d_{MC}^2 f_{A_{MC}} \tag{50}$$

$$f_{A_{MC}} = exp\left[-\frac{0.1335}{1+2.225\ln^2(d_{MC}/d_C)}\right] \tag{51}$$

where the correction factor f_{AMC} is empirical, with the correct properties of becoming one when the droplet is very large in globular transfer, or when the droplet is very small in spray transfer. At the transition from globular to spray, when the droplet has the same diameter as the molten consumable, it has a value of 0.875, which is the intermediate between subtracting the cross sectional area of the consumable (as should be done in globular) and not (as is the case of spray). When the droplet has twice the diameter of the

consumable (chosen as a representative globular transfer situation), this function has the value of 0.9375, corresponding to subtracting the full cross sectional area of the consumable. This approximation does not consider the evolution of surface area as the droplet forms, it only considers the geometry present at detachment, which is an overestimation; conversely, it might underestimate the evaporation area in spray transfer mode in the case there is a long molten tail.

COMPONENTS OF ENERGY BALANCE

HEAT BY ADVECTION

Advection is the transport of thermal energy due to the transport of mass. All mass flows involved in the mass balance also represent heat flows according to the following relationship

$$q_{adv} = \dot{m}h \tag{52}$$

where q_{adv} is the heat transported by advection across the surface of the control volume, $\dot{m}$ is the mass rate transporting heat across the surface of the control volume, and h is the enthalpy of the mass crossing the surface of the control volume. Similarly to temperature, enthalpy has an arbitrary reference point which is the same for all enthalpies considered. This equation recognizes that the temperature of the wire is uniform through its cross section. This hypothesis is quite accurate in GMAW except for the region surrounding the point of electrical contact between the wire and the contact tip, which might experience significant local gradients, especially with pulsed current, but this is not a problem because the control volume can be considered to start far upstream from the point of contact, and the exit part of the control volume is also far from the contact point. The hypothesis of uniform temperature might not be accurate in the exit region of the control volume in the case of tubular wires (e.g. MCAW, FCAW), in which the heat generated in the sheath might not propagate to the core of the wire by the time melting is reached.

Considering that the temperature of the wire is uniform across its cross section as it enters the control volume, the heat into the control volume by advection is

$$q_{adv_{in}} = \dot{m}_C h_C \tag{53}$$

where h_C is the enthalpy of the wire at the temperature it enters the control volume (typically room temperature).

The heat out of the control volume by advection is

$$q_{adv_{out}} = q_{MC} + q_V \tag{54}$$

where q_{MC} is the energy lost as molten metal in the form of droplets and spatter, and q_V is the energy lost as metal vapors.

Considering the average temperature of the molten metal exiting the control volume we obtain

$$q_{MC} = \dot{m}_{MC} h_{MC} \tag{55}$$

where h_{MC} is the average enthalpy of the molten metal, i.e. the average droplet temperature and spatter from the electrode assuming it exits at the same temperature of the droplet. The heat carried out by the metal vapors is

$$q_V = \dot{m}_V h_V \tag{56}$$

where h_{V} is the average enthalpy of the metal vapors.

Replacing into Eq. 17 we obtain

$$q_{adv_{out}} = \dot{m}_C h_C - \dot{m}_{MC} h_{MC} - \dot{m}_V h_V \tag{57}$$

Using Eq. 7 we can write

$$q_{adv_{tot}} = -[\dot{m}_C (h_{MC} - h_C) + \dot{m}_V (h_V - h_{MC})] \tag{58}$$

This equation means that the overall effect of advection takes thermal energy away from the control volume, and that the energy exiting has two components: first, the amount of heat used to raise the wire temperature from its starting temperature in solid state to the average temperature of the molten metal at the electrode tip, and the second component is the amount of energy needed to vaporize a (small) fraction of the consumable. This vaporization is the main source of the undesirable welding fumes and black deposits on the base metal when using Al-Mg consumables.

Enthalpies associated with melting the wire

Fig. 6 illustrates the enthalpies associated with metal from the wire, from the moment it leaves the spool to the moment is molten or evaporated.

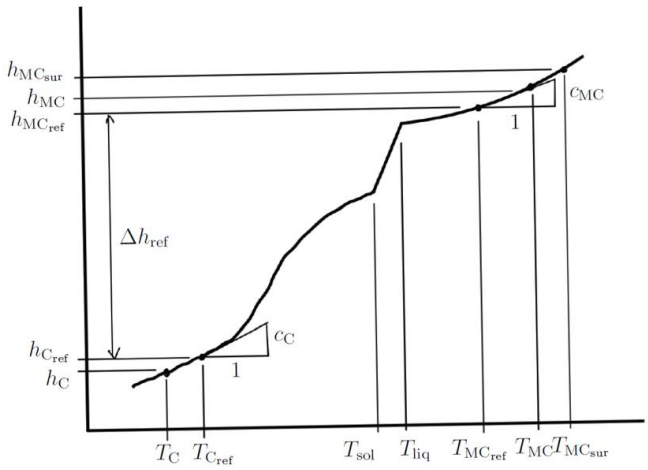

Fig. 6 Enthalpies associated with melting the wire in GMAW

The wire leaves the spool at temperature T_{spool}, typically the temperature of the environment, of the order of 20°C in a workshop. The wire enters the control volume with enthalpy h_C, corresponding to T_C. Typically, there is no preheating of the wire before it reaches the contact tip; so under normal conditions

$$T_C = T_{spool} \tag{59}$$

where the enthalpy corresponding to T_C is h_C. As the wire heats up inside the control volume, enthalpy increases in the form of sensible heat associated with a specific heat, and latent heat associated with transformations such as melting and solid state transformations such as austenization in steel wires. By the time the droplet (or spatter) exits the control volume, the average enthalpy of the molten metal is h_{MC}, associated with temperature T_{MC}, which is of the order of 2500°C in steel and 2200°C in aluminum wires [13,14,37,38].

Enthalpies associated with vaporization

The metal vapors exit the control volume at the same temperature of the surface of the droplet, it is not necessary to reach boiling temperature to evaporate; however, the latent heat of vaporization is still present and must be accounted for. Accounting for the mass rate of the different alloying elements (equation 22), Eq. 56 can be rewritten as

$$q_V = \sum_j \dot{m}_{V_j} h_{V_j} \tag{60}$$

and the average enthalpy of metal vapors can then be calculated as

$$h_V = \frac{\sum_j \dot{m}_{V_j} h_{V_j}}{\dot{m}_V} \tag{61}$$

For each evaporating alloying element, its enthalpy can be calculated as

$$h_{V_j} - h_{MC} = (h_{MC_{sur}} - h_{MC}) + (h_{V_j} - h_{MC_{sur}}) \tag{62}$$

where h_{Vj} and h_{MCsur} correspond to the temperature of the surface of the droplet, and their magnitude is the latent heat of vaporization of metal vapor j at the temperature T_{MCsur}. Thus:

$$h_{V_j} - h_{MC_{sur}} = h_{lg} \tag{63}$$

where h_{lgj} is tabulated, typically at the boiling temperature at atmospheric pressure. The dependence of latent heat of vaporization with the temperature of vaporization is negligible, and seldom tabulated. Equation 58 can then be rewritten as

$$q_{adv_{tot}} = -\dot{m}_C(h_{MC} - h_C) - \dot{m}_V[h_{lg} + (h_{MC_{sur}} - h_{MC})] \tag{64}$$

Where h_{lg} is the average enthalpy of vaporization for all metal vapors:

$$h_{lg} \approx \frac{\sum_j \dot{m}_{V_j} h_{lg_j}}{\dot{m}_V} \tag{65}$$

Practical expression of enthalpies for calculations

In welding, metals experience transformations in solid state, melting, and vaporization; for this reason, it is not practical to calculate enthalpies based on tabulated specific and latent heats. We can take advantage of the fact that in welding, metals start in solid state at temperatures typically not far from room temperature, and melt to relatively high temperatures, but in a relatively narrow range. We can select

$$T_{C_{ref}} = 20°C \tag{66}$$

as reference temperature in the solid for all metals. The temperature T_{MCref} is the reference temperature for the molten metal. For steel we will use 2500°C, for Aluminum 2200°C. For other alloys we will use a round number close to $0.9T_{\mathrm{boil}}$, where the temperatures must be in K, and T_{boil} is the boiling temperature of the base element of the alloy. If more than one element can be considered the solvent (because they have similar amounts in the alloy), we will choose the one with lower boiling temperature.

The reference temperatures correspond with the enthalpies h_{rfsol} and h_{MCref}, with the following enthalpy change:

$$h_{MC_{ref}} - h_{C_{ref}} = \Delta h_{ref} \tag{67}$$

Because the reference temperatures are close to the actual temperatures involved, all latent heats associated with melting and phase transformations are included in Δh_{ref}. The difference between Δh_{ref} and the factor ($h_{\mathrm{MC}} - h_{\mathrm{C}}$) required in Eq. 64 is due only to sensible heats, which are captured accurately near the reference points by the corresponding specific heats of solid and liquid c_{C} and c_{MC} evaluated at the reference temperatures. This way:

$$h_{MC} - h_C \approx \Delta h_{ref} + c_{MC}\,(T_{MC} - T_{MC_{ref}}) - c_C(T_C - T_{C_{ref}}) \tag{68}$$

Similarly, ($h_{\mathrm{MCsur}} - h_{\mathrm{MC}}$) required in Eq. 64, can be estimated as

$$h_{MC_{sur}} - h_{MC} \approx c_{MC}(T_{MC_{sur}} - T_{MC}) \tag{69}$$

Using the accurate approximations above, the exact calculation of overall heat transferred by advection (equation 58) can be expressed as:

$$q_{adv,tot} \approx -\dot{m}_C[\Delta h_{ref} + c_{MC}(T_{MC} - T_{MC_{ref}}) - c_C(T_C - T_{C_{ref}})] - \dot{m}_V[h_{lg} + c_{MC}(T_{MC_{sur}} - T_{MC})] \tag{70}$$

where the first term on the right of the equation accounts by the energy absorbed by the molten consumable, and the second term accounts for the energy absorbed by vaporization. For then experiments performed in steels, vaporization absorbs less than 1.5% of the total energy, while in aluminum the amount of energy absorbed by the vapors

is about 6% in average, reaching just above 10% in some cases. There is no large difference in the energy absorbed for different alloys.

Experiments show that the temperature of the molten metal in the droplet is fairly uniform [39], such that the temperature of the surface of the droplet where evaporation occurs is not far from the average temperature of the droplet. Because the gradient inside the droplet can be expected to be shallow, the term containing the factor ($T_{\mathrm{MCsur}} - T_{\mathrm{MC}}$) is typically negligible.

HEAT FROM ARC COLUMN

In the heat exchange between the arc and the electrode, convection dominates over radiation.

$$q_{AC,C} = h_{AC,C} A_{AC,C} (T_{AC_{MC}} - T_{MC_{surf}}) \tag{71}$$

This exchange happens at the area of attachment of the arc to the electrode, which in the case of globular transfer can be estimated using Eq. 20, and for the case of spray transfer will be approximate as the area of the droplet using Eq. 50.

The estimation of convection coefficient is typically based on tabulations of the Nusselt number. In this case, the Nusselt number can be approximated using the heat transfer correlation for a sphere in an external flow [30], similarly as it was done for mass transfer:

$$h_{AC,C} = \frac{k_{AC_{MC}} Nu_{AC,C}}{d_{MC}} \tag{72}$$

$$Nu_{AC,C} = 2 + 0.6 Re_{AC}^{1/2} Pr_{AC}^{1/3} \tag{73}$$

$$Pr_{AC} = \frac{\nu_{AC}}{\alpha_{AC}} \tag{74}$$

For the plasma properties, the temperature considered is the same as for the case of mass diffusion (5000 K for Ar). Tor the experiments performed, $h_{\mathrm{AC,C}}$ is of the order of 10^3 $\mathrm{Wm^{-1}K^{-1}}$, $v_{\mathrm{AC,C}}$ is between 5 and 8, indicating that advection dominates over conduction, but not by much. the value of Pr at 5000 K is approximately 0.6.

HEAT FROM CONTACT TIP TO CONSUMABLE

The consumable touches the contact tip typically at the entrance and at the exit of the contact tip. There is heat exchange through these two points of contact, and also between the inner surface of the contact tip bore and the outer surface of the consumable traversing through the contact tip.

The two points of contact transfer heat differently. The contact at the exit of the contact tip carries the almost all the current, and experiences Joule heating related to the electrical resistance of contact. The contact at the entrance of the contact tip experiences negligible

Joule heating, and its heat exchange is included in the calculation of heat exchange between the surfaces of the contact tip and wire. Thus

$$q_{CT,C} = q_{CT,C_{cont}} + q_{CT,C_{gap}} \tag{75}$$

where $q_{\mathrm{CT,C}}$ is the total heat exchanged between the contact tip and the consumable, $q_{\mathrm{CT,Ccont}}$ is the heat exchange by contact at the exit of the contact tip, and $q_{\mathrm{CT,Cgap}}$ is the heat exchanged across the gap between the inner surface of the contact tip bore and the outer surface of the electrode. For the experiments performed, $q_{\mathrm{CT,C}}$ is of the order of 30 W, $q_{\mathrm{CT,Ccont}}$ is only a fraction of $q_{\mathrm{CT,Cgap}}$, of the order of 15% or less for the case of aluminum alloys, and up to 50% in the case of steels. In aluminum, the flow of $q_{\mathrm{CT,Ccont}}$ is estimated to be from the hot contact to the electrode; however, in steels, the consumable at the point of contact can be very hot, and $q_{\mathrm{CT,Ccont}}$ flows from the electrode towards the contact tip.

Heat by conduction across the main point of electrical contact

Both the wire and the contact tip are locally hotter at the main point of electrical contact; however these peak temperatures are different, causing heat to be transferred across the main point of electrical contact. While the peak temperature of the consumable at the electrical contact can be substantially higher than the temperature of the spool, in the absence of intense pulsing, we will assume that the contact tip is at an approximately uniform temperature.

Assuming that the contact tip is hotter than the consumable at the point of electrical contact, the heat transferred across the contact is

$$q_{CT,cont} = \frac{T_{CT} - T_{C_{cont}}}{\mathcal{R}_{CT,C_{cont}}} \tag{76}$$

where $\mathcal{R}_{CT,C_{cont}}$ is the thermal resistance of contact between consumable and the contact tip, T_{CT} is the temperature of the contact tip (assumed uniform, typically 350°C [40,41]), and T_{Ccont} is the temperature of the consumable at the point of electrical contact.

To calculate the thermal resistance of contact, we can consider only the dominant component, which is conduction through asperities, neglecting the conduction and radiation through the air in the gaps. In this case, an analogy can be established between the electrical and thermal contact resistances, based on the fact that both contact resistances share the same geometric features at the point of contact. Thus:

$$\mathcal{R}_{CT,C_{cont}} = \frac{k_{CT}^{-1} + k_{C}^{-1}}{\varrho_{CT} + \varrho_{C}} R_{CT,C_{cont}} \tag{77}$$

Considering the properties of Table 1, and a representative contact resistance of 1 mΩ for copper coated consumables and aluminum, Equation 77 indicates a thermal contact resistance at the point of electrical contact of 87 KW^{-1} for copper coated consumables, and 76 KW^{-1} for aluminum consumables.

The temperature of the consumable at the point of contact can be estimated approximately as

$$T_{C_{cont}} = T_C + \mathcal{R}_{C_{cont}} q_{C_{cont}} \tag{78}$$

where q_{Ccont} is the amount of Joule heating generated on the consumable at the point of contact, calculated in Eq. 84 below.

Table 1 Thermal and electrical properties of the contact tip and consumables

	k W m^{-1}K^{-1}		ϱ Ω m	
Cu coating	394	†	$3\,10^{-8}$	‡
Steel	41		$7\,10^{-7}$	
Aluminum	229	*	$6\,10^{-8}$	
Contact tip	300	§	$3.75\,10^{-8}$	§

† annealed copper at 200°C [42], ‡ [43], * [44], § Cu Cr Zr tip

The thermal resistance of the consumable at the main point of electrical contact can be estimated using the distributed moving heat source analysis in [45]:

$$\mathcal{R}_{C_{cont}} = 1.13\ \frac{1}{k_C}\sqrt{\frac{\alpha_C}{L_{cont}^3 U_C}} \tag{79}$$

where $\mathrm{RC}_{\mathrm{cont}}$ is the thermal resistance of the consumable at the area of contact, based on the maximum temperature of the consumable at the area of contact $T\mathrm{C}_{\mathrm{cont}}$, a square contact, and a uniform distribution of heat flux at the point of contact. The parameter U_{C} is wire feed speed, L_{cont} is the side length of the square that defines the area of contact, and k_{C} and α_{C} are the thermal conductivity and diffusivity of the consumable at a temperature representative of the area of contact. The thermal resistance of a moving heat source involves the penetration of heat under the surface of the consumable to depths much larger than the thickness of a copper coating, thus the effect of copper coating will be neglected. The value of $\mathrm{RC}_{\mathrm{cont}}$ has little dependence (less than 25%) on the exact shape of the area of contact or the distribution of heat, so the assumption of a square contact or uniform heat flux are not critical for this analysis. For the experiments performed, the value of $\mathrm{RC}_{\mathrm{cont}}$ did not vary much, with an average around 20 KW^{-1} for steels, and 12 KW^{-1} for aluminum consumables.

The maximum temperature of the consumable at the contact point is important, because if there is localized melting the consumable can weld itself to the contact tip and cause very fast degradation of the contact tip. This problem is especially relevant in the case of pulsed current, where the peak current can be very high (resulting in high q_{Ccont}), and the wire feed speed is relatively low for that high current (resulting in high $\mathrm{RC}_{\mathrm{cont}}$). For the experiments performed, T_{Ccont} was estimated to range between 240°C and 800°C for steels, and 65°C and 400°C in aluminum consumables.A reasonable intermediate choice for temperature at which to evaluate the consumable properties is the average between the maximum temperature at the area of contact and the consumable temperature $T_{\mathrm{Ccont,ave}}$ calculated as:

$$T_{C_{cont,inter}} = T_C + 0.5(\hat{T}_{C_{cont}} - T_C) \tag{80}$$

Where $\hat{T}_{C_{cont}}$ is obtained from Eq. 79 and Eq. 78 using the consumable properties corresponding to T_C. The size of L_{cont} depends on the consumable size, the gap with the contact tip, the pressure at the point of contact (related to the cast of the wire), and the amount of wear; a reasonable estimate based on experience is

$$L_{cont} = 0.4 d_C \tag{81}$$

The flow of heat $q_{CT,Ccont}$ is quite small for two reasons. First, the thermal resistance at the point of sliding contact is substantially higher than the thermal resistance of the wire. Also, because the temperature difference between the contact tip and the surface of the consumable is small. The small value of $q_{CT,Ccont}$ allows the calculation of T_{Ccont} in Eq. 78 neglecting the heat flux by contact.

Heat across the gap between contact tip and consumable

Outside the main point of electrical contact, the contact tip and the consumable will exchange energy by radiation and conduction across the thin gap between them. Assuming that the contact tip is hotter than the consumable at the point of electrical contact, the heat transferred across the contact is

$$q_{CT,C_{gap}} = \frac{T_{CT} - T_C}{\mathcal{R}_{CT,C_{gap}}} \tag{82}$$

where T_C is the temperature of the consumable outside the point of electrical contact and $\mathcal{R}_{CT,C_{gap}}$ is the thermal resistance of the gap between consumable and the contact tip and can be estimated as

$$\mathcal{R}_{CT,C_{gap}} = \frac{1}{\pi^2} \frac{\Delta d_{CT,C}}{d_C L_{CT} k_{gap}} \tag{83}$$

where $\Delta d_{CT,C}$ is the difference in diameters between the consumable and the bore in the contact tip, d_C is the diameter of the consumable, L_{CT} is the length of the contact tip bore, and k_{gap} is the thermal conductivity of the fluid in the gap between the consumable and the contact tip bore (typically air). A representative value of $\mathcal{R}_{CT,C_{gap}}$ is 10 K W $^{-1}$. A representative temperature for the consumable is 20°C, and for the contact tip 350°C [40,41], resulting in a heat rate $q_{CT,Cgap} \approx 30$ W.

JOULE HEATING GENERATED AT THE MAIN POINT OF ELECTRICAL CONTACT

The Joule heating generated at the point of electrical contact can be estimated as

$$q_{C_{cont}} = f_{C_{cont}} q_{cont_{Joule}} \tag{84}$$

where $q_{contJoule}$ is the total amount of Joule heating generated at the main point of electrical contact, and f_{Ccont} is the fraction of that heat absorbed by the consumable. This overall heat generated at the point of contact is calculated as

$$q_{cont_{Joule}} = I^2 R_{cont} \tag{85}$$

where I is the RMS current, and R_{cont} is the contact resistance at the point of sliding contact, typically of the order of 1 mΩ. Assuming that the geometry of electrical conduction through the asperities is symmetrical across the line of contact between the contact tip and then consumable, the fraction of overall Joule heating generated at the contact by the consumable is

$$f_{C_{cont}} = \frac{\varrho_{C_{cont,ave}}}{\varrho_{C_{cont,ave}} + \varrho_{CT}} \tag{86}$$

where $\varrho_{C_{cont,ave}}$ is the electrical resistivity of the consumable surface at the average temperature at the point of contact. For a square contact with a uniform heat distribution, the average surface temperature is [45]:

$$T_{C_{cont,ave}} = T_C + 0.667(T_{C_{cont}} - T_C) \tag{87}$$

Typical values of f_{Ccont} are 0.44 for copper coated wires, 0.88 for non-coated steel wires, and 0.63 for aluminum wires.

JOULE HEATING FROM ELECTRODE EXTENSION

The energy generated at the electrode extension by Joule heating (q_{EE}) can be calculated as

$$q_{EE} = \frac{\varrho_{eff} L I^2}{A_C} \tag{88}$$

where ϱ_{eff} is the effective resistivity of the electrode extension, L is the length of the electrode extension (time averaged for globular), and A_{c} the cross-sectional area of the wire. Following [46], the electrode extension is considered the length of electrode between the exit point of the contact tip and the point of arc attachment illustrated in Fig. 5. The effective resistivity in typical conditions can be calculated with accuracy using the expressions in [15]:

$$\varrho_{eff} = \varrho_0 M_1 \left[2 \frac{\gamma - 1}{b(1-\gamma) + d(1+\gamma)} \right] \tag{89}$$

$$M_1 = \frac{\rho \Delta h_{0,sol} U_C A_C^2}{\varrho_0 I^2 L} \tag{90}$$

$$\gamma = exp(d/M_1) \tag{91}$$

$$d = \sqrt{b^2 - 4a} \tag{92}$$

$$a = -4\Delta\varrho_2/\varrho_0 \tag{93}$$

$$b = (\Delta\varrho_1 + 4\Delta\varrho_2)/\varrho_0 \tag{94}$$

where ϱ_0 is the electrical resistivity at the wire spool temperature (assumed 20°C), $\Delta\varrho_1$ is the variation in resistivity between the spool temperature and solidus, $\Delta\varrho_2$ is the maximum departure from linear in the variation in resistivity, indicated with vertical segments in Fig. 7, using aluminum alloys as examples. The symbol ρ corresponds to the wire density at room temperature, $\Delta h_{0,sol}$ is the variation in enthalpy between spool temperature and solidus, A_c is the cross sectional area of the wire, based on wire diameter d_c, and L is the length of electrode extension. The value of ϱ_{eff} varies only slightly with the operating conditions for aluminum, between 3.0 10^{-8} Ωm and 3.5 10^{-8} Ωm for all aluminum alloys under all conditions, and varying more widely in ER80S-G, from 2.6 10^{7} Ωm to 4.5 10^{7} Ωm.

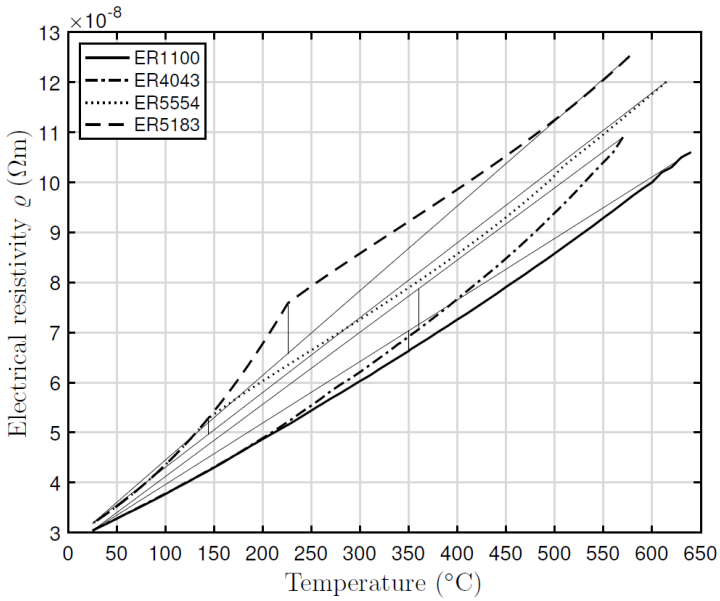

Fig. 7 Electrical resistivity of aluminium alloys tested

HEAT FROM OVERALL FALL VOLTAGE

Most of the heat that melts the electrode comes from the overall fall voltage at the electrode often captured as:

$$q_{elec_{over}} = IV_{elec_{over}} \tag{95}$$

Where $V_{elec_{over}}$ depends only weakly on the welding current. Typically the electrode is positive, making the electrode an anode. In this case, the anode voltage consists of three components

$$V_{elec_{over}} = V_{an_{over}} = V_{an_{fall}} + \phi_{an} + \frac{3}{2}\frac{k_B}{e}T_{AC_{MC}} \quad (96)$$

where $V_{an_{fall}}$ is typically called the "anode fall," associated with the non-equilibrium parts of the plasma, φ_{an} is the work function of the anode material (the surface of the consumable over the area of arc attachment), and the last term captures the energy deposited by the electrons as they condense on the electrode. The temperature $T_{AC_{MC}}$ is the temperature of the electrons that deposit on the electrode, of the order of 7300 K for Ar.

The work function is a measure of the energy required to extract an electron from the surface of a solid or liquid cathode. The work function is not a characteristic of a bulk material, but a property of the surface of the material. The work function of crystalline metals often varies by about 10% between different surfaces of the same single crystal, and the work function of molten metal is undistinguishable from that of polycrystalline solid [47]. A reasonable approximation for the effective work function of an alloy (ϕ_{eff}) can be obtained by using the rule of mixtures:

$$\phi_{eff} = \sum_i f_{mol_i}\phi_i \quad (97)$$

Where f_{mol_i} is the molar fraction of alloying component *i* on the surface, and ϕ_i is its corresponding work function. The effective work function is often undistinguishable from that of the base alloy element. The anode voltage fall is influenced by the size of the arc attachment, the plasma velocity around it, and the presence of metal vapors.

Fig. 8 illustrates the anode fall voltages associated with the experiments performed. The markers correspond to each experiment performed, and the trendlines are two-point moving averages. The lowest horizontal line corresponds to $\frac{3}{2}\frac{k_B}{e}T_{AC_{MC}}$ in Equation 96 for 7300 K (0.944 V). The multiple closely-packed horizontal lines correspond to $\phi_{an} + \frac{3}{2}\frac{k_B}{e}T_{AC_{MC}}$. The small dispersion is due to the different estimated work functions for the different alloy compositions. It can be seen that consumable composition does not change the effective work function far from the value of the solvent. The difference between the trendlines and the highest horizontal lines corresponds to $V_{an_{fall}}$, which varies from -1 V to 2 V in the current interpretation of results. The negative value is unlikely, and is discussed in the Discussion section.

HEAT GENERATION AT THE MOLTEN CONSUMABLE

The electrode extension ends at the droplet in globular transfer, and at the attachment of the arc in spray transfer (which is approximately coincident with the start of melting). This section beyond the electrode extension will be called the "molten consumable" section. Current flowing thorough the molten consumable section generates heat that can be calculated as

$$q_{MC_{Joule}} = I^2 R_{MC} \quad (98)$$

In globular transfer the resistance can be estimated assuming the path of current inside the current is a truncated cone, from the electrode cross section to the arc attachment. The shape of the droplet changes as it grows, and a time average of this resistance results in

$$R_{MC_{glob}} = \frac{3}{4}\frac{\varrho_{MC} d_{MC}}{A_C}\frac{d_C}{2L_{AC,MC}} \tag{99}$$

where the ratio on the right of the equation is typically not far from 1.

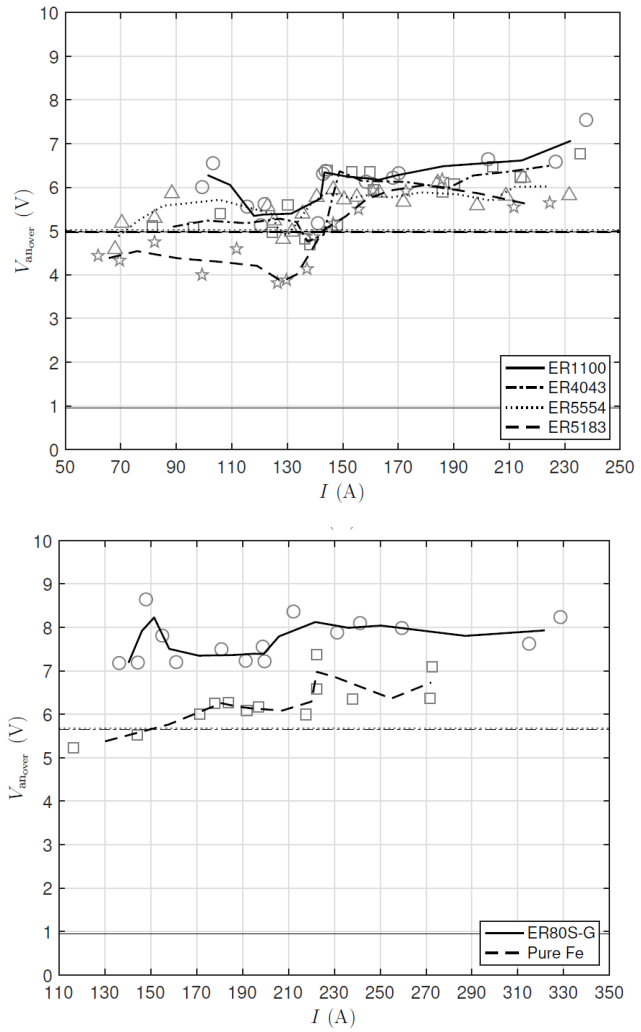

Fig. 8 Anode fall estimated in experiments performed. Markers indicate independent measurements, and trendlines correspond to a moving average of two points.

In spray transfer, the tapered electrode can be approximated as having a length of the order of the electrode diameter, and a thickness of the neck of the order of half an electrode diameter. Because much current flows through the taper, and the droplet is completely enveloped by the arc, it will be considered that only the taper contributes to Joule heating, resulting in

$$R_{MC_{spray}} = 2\frac{\varrho_C d_C}{A_C} \tag{100}$$

where the resistivity of the consumable corresponds to the melting temperature. Equations 99 and 100 can be blended as an approximation, resulting in

$$R_{MC} = R_{MC_{glob}} + \frac{R_{MC_{spray}} - R_{MC_{glob}}}{1+\left(\frac{d_{MC}}{d_C}\right)^n} \tag{101}$$

where the value of n is determined empirically. A reasonable value is n = 4.248, which results in a 95% approximation to the asymptotic value when the droplet diameter is twice or half that of the consumable. Typical values of $R_{MC_{glob}}$ are of the order of 1 mΩ for steels and 0.3 mΩ for aluminum, and typical values of $R_{MC_{spray}}$ are approximately a third of those.

DISCUSSION

This analysis indicates confirms previous findings in [8] that the electrode extension is not influential in aluminum consumables, and that the higher in deposition rate in Mg-containing aluminum alloys are due to their lower droplet temperature, and not their higher resistivity.

This analysis also confirms the hypothesis of [3] in which heat losses by evaporation are small, of the order of 100 W or lower. This small value is still important for an accurate determination of anode fall voltage.

The main source of error in this analysis is associated with the geometry of the electrode tip. A systematic study with high-quality images is necessary to provide an appropriate description of electrode geometry. For droplet detachment frequency measurements, it is recommended to measure the time between a large number of detachments observed in a video capture; for 10 detachments the error would be of the order of 10%, and for 100 detachments, of the order of 1%. The determination of frequency can be accelerated with the use of machine learning, as described in [48].

The negative values of anode fall voltage obtained in Fig. 8 for the globular range are unlikely. One possible source of this surprising result is that evaporation in the globular regime is underestimated. The hypothesis of uniform droplet temperature might need to be reassessed accounting for higher temperatures at the bottom of the droplet, as originally proposed in [49].

The analysis presented can be extended in a straightforward way to other alloys such as stainless steels to estimate the rate of evaporation of Cr. It can also be extended without much difficulty to other wire-based processes such as SAW, FCAW, and MCAW, and

can constitute the basis for an analysis of SMAW. This extension is not without challenges, but the theoretical basis is established.

CONCLUSIONS

This work presents a complete mass and energy balance of GMAW with solid wire. For the first time, the mass transfer associated with evaporation of a real alloy and its many elements is considered. In contrast with most previous work in which only Langmuir-type evaporation is considered, the resistance to mass transfer in the liquid and gas phases is considered, and it is found that the dominant mechanism in alloy evaporation is diffusion in the gaseous boundary layer. This conclusion is novel and provides explanations to observed phenomena such as the increased fume formation when using reactive gases, which reduce the thickness of the boundary layer.

The value of the anode fall in spray transfer is determined to be of the order of 1 V to 2 V both in steel and aluminum alloys. The estimated value of anode fall voltage in globular transfer varies from -1 V to 2 V. The low and negative values are likely due to the underestimation of evaporation in the globular regime.

This analysis, together with the estimation of anode fall voltage, provides a general way of estimating deposition rate and fume formation rate in any alloy, not just steels and aluminum. This capability is important especially in the field of additive manufacturing, in which new alloys uncommon in welding are explored, and understanding of deposition rate is essential for controlling layer height.

ACKNOWLEDGEMENTS

The authors would like to acknowledge Prof. Tanaka of Osaka University for the generous gift of a roll of pure iron consumable.

References

[1] A. LESNEWICH: ‘Control of melting rate and metal transfer in gas-shielded metal-arc welding part i - control of electrode melting rate’, *Welding Journal*, pages 343s–353s, 1958.

[2] E. HALMOY: ‘Wire melting rate, droplet temperature, and effective anode melting potential’, In: W. Lucas, editor, *Arc Physics and Weld Pool Behaviour*, volume 1, pages 49-57, The Welding Institute, 1979.

[3] J. H. WASZINK and G. J. P. M. VAN DEN HEUVEL: ‘Heat generation and heat flow in the filler metal in GMA welding’, *Welding Journal*, pages 269s-282s, 1982.

[4] G. HUISMANN and H. HOFFMEISTER: ‘Sensing metal inert gas process by measuring wire feedrate and current’, *Science And Technology Of Welding And Joining*, 4(6):352-356, 1999.

[5] M. EBERT-SPIEGEL, S.-F. GOECKE and M. RETHMEIER: ‘Possibilities for compensating a higher heat input, in particular by the torch offset relative to the top sheet at the fillet weld on a lap joint’, *Welding in the World*, 59(3):443-453, 2015.

[6] YL CHANG and AS BABKIN: ‘Calculation of solid wire melting rate in co2 welding’, *Welding Journal*, 95(5):163-173, 2016.

[7] LINCOLN ELECTRIC: *Gas metal arc welding. product and procedure selection*, Report C4.200, Lincoln Electric, 2014.

[8] Z. YAN, K. S. SCOTT, S. CHEN and P. F. MENDEZ: 'Deposition rate in gmaw of ER1100 and ER5183 aluminum alloys', *Welding Journal*, 101:289s-292s, 2022.

[9] E. SODERSTROM, K. M. SCOTT and P. F. MENDEZ: 'Calorimetric measurement of droplet temperature in GMAW', *Welding Journal*, 90(4):77s-84s, 2011.

[10] K. M. SCOTT: *Heat transfer and calorimetry of tubular ni/wc wires deposited with gmaw*, 2011.

[11] J. CHAPUIS, K. M. SCOTT, St. D. GUEST, E. SODERSTROM and P. F. MENDEZ: 'Temperature and Size Measurements of Droplet During Free Flight Gas Metal Arc Welding (Mesures de temp´erature et de taille de goutte en vol libre lors d'une op´eration de soudage MIG-MAG)', In: *Canadian Welding Association Annual Conference*, 2011.

[12] J. CHAPUIS, K. M. SCOTT, St. D. GUEST, E. SODERSTROM and P. F. MENDEZ: 'Droplet calorimetry and high speed videography of free flight metal transfer in gas metal arc welding', In: *IIW Annual Assembly*, pages Doc.212-1232-12, 2012.

[13] C. MCINTOSH, J. CHAPUIS and P. F. MENDEZ: 'Effect of ar-co2 gas blends on droplet temperature in gmaw', *Welding Journal*, 95(8):273s-279s, 2016.

[14] C. MCINTOSH and P. F. MENDEZ: 'Fall voltages in advanced waveform aluminum GMAW', *Welding Journal*, 96:354s-366s, 2017.

[15] G. LEHNHOFF and P. F. MENDEZ: 'Scaling of non-linear effects in heat transfer of a continuously fed melting wire', *International Journal of Heat and Mass Transfer*, 54:2651-2660, 2011.

[16] A. SCOTTI, V. PONOMAREV and W. LUCAS: 'A scientific application oriented classification for metal transfer modes in gma welding', *Journal of materials processing technology*, 212(6):1406-1413, 2012.

[17] J NORRISH: 'A review of metal transfer classification in arc welding' (iiw doc. xii-1769-03. bucharest), *Villepinte, France: International Institute of Welding*, 2003.

[18] A. BLOCK-BOLTEN and T. W. EAGAR: 'Metal vaporization from weld pools', *Metallurgical Transactions B*, 15B:461-469, 1984.

[19] C. B. ALCOCK, V. P. ITKIN and M. K. HORRIGAN: 'Vapour pressure equations for the metallic elements: 298–2500k', *Canadian Metallurgical Quarterly*, 23(3):309-313, 1984.

[20] D. R. LIDE: *CRC handbook of chemistry and physics*, volume 85. CRC press, 88 edition, 2008.

[21] P KUBÍČEK and T PEPŘICA: 'Diffusion in molten metals and melts: application to diffusion in molten iron', *International metals reviews*, 28(1):131-157, 1983.

[22] K. UEMURA: 'The diffusion of various elements into aluminium in molten state (i)', *Tetsu-to-Hagane*, 25(1):24-29, 1939.

[23] K. UEMURA: 'The diffusion of various elements into aluminium in molten state (ii)', *Tetsu-to-Hagan´e*, 26(11):813-816, 1940.

[24] J. B. EDWARDS: *Diffusion in binary liquid-metal systems*, 1968.

[25] A. K. ROY and R. P. CHHABRA: 'Prediction of solute diffusion coefficients in liquid metals', *Metallurgical Transactions A*, 19(2):273-279, 1988.

[26] E. T. TURKDOGAN, P. GRIEVESON and L. S. DARKEN: 'The formation of iron oxide fume', *JOM*, 14(7):521-526, 1962.

[27] E. T. TURKDOGAN, P. GRIEVESON and L. S. DARKEN: 'Enhancement of diffusion-limited rates of vaporization of metals', *The Journal of Physical Chemistry*, 67(8):1647-1654, 1963.

[28] St. E. FERREE: 'New generation of cored wires creates less fume and spatter', *Welding journal*, 74(12):45-49, 1995.

[29] K. R. CARPENTER, B. J. MONAGHAN and J. NORRISH: 'Influence of shielding gas on fume formation rate for gas metal arc welding of plain carbon steels', In: *Trends in Welding Research*, pages 436-442, 2009.
[30] T. BERGMAN, A. LAVINNE, F. INCROPERA and D. DEWITT: *Introduction to Heat Transfer*, John Willey and Sons, New Jersey, United States, sixth edition, 2002.
[31] C. J. REDDING: 'Fume model for gas metal arc welding', *Welding Journal-New York-*, 81(6):95-S, 2002.
[32] A. B. MURPHY and C. J. ARUNDELL: 'Transport coefficients of argon, nitrogen, oxygen, argon-nitrogen, and argon-oxygen plasmas', *Plasma Chemistry and Plasma Processing*, 14:451-490, 1994.
[33] P. F. MENDEZ, M. A. RAMIREZ, G. TRAPAGA and T. W. EAGER: 'Order-of-magnitude scaling of the cathode region in an axisymmetric transferred electric arc', *Metallurgical And Materials Transactions B-Process Metallurgy And Materials Processing Science*, 32(3):547-554, 2001.
[34] M. A. RAMIREZ: *Mathematical modeling of d. c. electric arc furnace operations*, 2000.
[35] A. B. MURPHY: 'Calculation and application of combined diffusion coefficients in thermal plasmas', *Scientific reports*, 4(1):1-5, 2014.
[36] C. R. REID, J. M. PRAUSNITZ and B. E. POLING: *The Properties of Gases and Liquids*. McGraw-Hill, 1987.
[37] C. MCINTOSH and P. F. MENDEZ: 'Experimental measurements of fall voltages in gas metal arc welding', *Welding Journal*, 96:121s-132s, 2017.
[38] V. ANDRÉS N. SÁNCHEZ: *Energy balance in gas metal arc welding*, 2021.
[39] E. SIEWERT, J. SCHEIN and G. FORSTER: 'Determination of enthalpy, temperature, surface tension and geometry of the material transfer in pgmaw for the system argon-iron', *Journal of Physics D: Applied Physics*, 46(22):224008, 2013.
[40] G ADAM, T. SIEWERT, T. QUINN and D VIGLIOTTI: 'Contact tube temperature during gmaw', (80), 2001-12-01 2001.
[41] D. E. KOLMOGOROV, S. A. SOLODSKY, L. B. GIL and V. I. BERG: 'Effect of various heat sources on heating of contact tip during mig/mag welding', In: *Materials Science Forum*, volume 927, pages 106-111. Trans Tech Publ, 2018.
[42] C. E. SCHUSTER, M. G. VANGEL, and H. A. SCHAFFT: 'Improved estimation of the resistivity of pure copper and electrical determination of thin copper film dimensions', *Microelectronics Reliability*, 41(2):239-252, 2001.
[43] J. R. DAVIS: *Concise metals engineering data book*, ASM international, 1997.
[44] Ø. GRONG: *Metallurgical Modelling of Welding*, Institute of Materials, Cambridge, Great Britain, 1st edition, 1994.
[45] Y. S. MUZYCHKA and M. M. YOVANOVICH: 'Thermal resistance models for non-circular moving heat sources on a half space', *Journal of Heat Transfer*, 123:624-632, 2001.
[46] St. EGERLAND: 'A contribution to arc length discussion', *Soldagem & Inspecao*, 20(3):367-380, 2015.
[47] R. EVANS: 'Surfaces. the surface properties of liquid metals', *Le Journal de Physique Colloques*, 41(C8):C8-775-C8-782, 1980.
[48] I. GONZÁLEZ PÉREZ, V. MERUANE and P. F. MENDEZ: 'Deep-learning based analysis of metal-transfer images in gmaw process', *Journal of Manufacturing Processes*, 85:9-20, 2023.
[49] P. F. MENDEZ, N. T. JENKINS and T. W. EAGAR: 'Effect of electrode droplet size on evaporation and fume generation in GMAW', In: *Gas Metal Arc Welding for the 21st Century*, pages 325-332, American Welding Society, 2000.